Solvent Extraction Flowsheet-Level Modeling and Simulation with Radiolysis

Valmor F. de Almeida*, Taha Azzaoui† and Kevin L. Lyon‡

*University of Massachusetts Lowell, Dept. of Chemical Engineering, Nuclear Program, Lowell, MA, 01854, USA, valmor_dealmeida@uml.edu, †University of Massachusetts Lowell, Dept. of Computer Science and Mathematical Sciences, Lowell, MA, 01854, USA, taha_azzaoui@student.uml.edu, and ‡Idaho National Laboratory, Aqueous Separations and Radiochemistry Group, Idaho Falls, ID, 83415, kevin.lyon@inl.gov, USA.

ABSTRACT

Flowsheet-level models do not account for explicilty coupled models of water, acid, The present work is aimed at developing an extensive flowsheet simulation capability using models for solvent extraction employed in cross-cutting applications in the area of nuclear separations, safeguards, materials protection, special materials for national security and non-proliferation, critical materials, mining, and metallurgy applications. Our approach takes into account participating aqueous, organic, and vapor phases, homogeneous and heterogeneous chemical reactions, coupled with radiolysis and hydrolysis of the aqueous and organic phases.

An important enabling component of the current development is the computational framework developed to allow for the dynamic coupling of multiple stages of solvent extraction. This parallel development named `Cortix` (`https://cortix.org` [1]) facilitates the time-coupling of multiple contacting stages or multiple contacting banks of typical solvent extraction equipment.

The purpose of this communication is to discuss the progress made thus far and to present preliminary results.

THEORY

This work considers the following reactive components for creating a combined reaction mechanism for nuclear solvent extraction using the commonly known tri-butyl-*n*-phosphate(TBP)/dodecane organic phase and nitric acid solution of actinides and fission products aqueous phase:

1. H_2O radiolysis [2],
2. HNO_3 radiolysis [3, 4, 2],
3. Actinides redox reactions [5],
4. Actinides complexation [6, 7],
5. H_2O complexation [8, 9],
6. HNO_3 complexation [6],
7. Tri-*n*-butyl phosphate hydrolysis [10, 4],
8. Tri-*n*-butyl phosphate radiolysis [4].

Radiolysis of the aqueous phase is an important ingredient for the speciation of many secondary components that react in both phases. Water radiolysis reaction mechanisms have been proposed for nuclear reactor accident conditions [2] which can be used as a starting point here. Strongly reactive reducing species are present, *i.e.* the solvated electron, $e^-_{(aq)}$, and the hydrogen atom, $H^\bullet$, in addition to the strongly oxidizing radical, $^\bullet OH$, and the hydrogen peroxide molecule, H_2O_2, of importance to various processes in used nuclear fuel aqueous reprocessing. An abbreviated representation of the primary water radiolysis reaction is

$$H_2O \overset{\gamma}{\rightsquigarrow} (2.7)\,{}^\bullet OH + (2.6)\,e^-_{(aq)} + (0.6)\,H^\bullet + (0.7)\,H_2O_2 + (2.6)\,H_3O^+ + (0.45)\,H_2,$$

where the G-values (in molecules per 100 eV) are given in parenthesis. Another 44 additional secondary reactions supplement the primary reaction, and another 10 acid/base reactions are added as additional secondary reactions involving a total of 18 species.

The primary nitric acid radiolysis reaction

$$NO_3^- \overset{\gamma}{\rightsquigarrow} (x)\,{}^\bullet NO_3 + (y)\,e^-_{(aq)},$$

produces nitrogen trioxide radical (a reactive compound that attacks ligands and organic diluents; more on this topic later) from dissociated nitric acid. The G-values are difficult to obtain from the literature as they depend on the nitric acid concentration and temperature (we use values estimated from [3]). Secondary reactions and additional nitrate reactions prompted by the radicals from water radiolysis follow the primary reaction for a total of 46 reactions and 17 species. Among them, HNO_2 couples acid radiolysis to redox reactions of actinides. Therefore this represents an additional source of oxidant. In particular, Pu^{3+} is oxidized to Pu^{4+} which makes partition from U^{6+} less productive in a TBP solvent extraction process. In addition, nitrous acid also disturbs the recovery of Np where the principal reactions from [5] are:

$$\begin{aligned}
Pu^{3+} + HNO_2 + H^+ &\xrightarrow{k_8} Pu^{4+} + NO + H_2O \\
2PuO_2{}^{2+} + HNO_2 + H_2O &\xleftrightarrow{k_9,k_{10}} 2PuO_2{}^{+} + NO_3^- + 3\,H^+ \\
2NpO_2{}^{+} + NO_3^- + 3H^+ &\xrightarrow{k_{20}} 2NpO_2{}^{2+} + HNO_2 + H_2O \\
2Np^{4+} + NO_3^- + 3H_2O &\xrightarrow{k_{21}} 2NpO_2{}^{+} + HNO_2 + 5H^+. \\
\vdots \quad + \quad \vdots &\longleftrightarrow \vdots \quad + \quad \vdots
\end{aligned}$$

The complete set of actinide redox reactions add 29 reactions and 19 species to the overall reaction mechanism.

Various complexation reactions take place at the interface of the organic and aqueous phases where TBP is active as a surfactant. We consider these interfacial reactions in the framework of mass transfer where the equilibrium distribution values are used to drive complexes across the interface for

a given (measured or estimated) relaxation time. We take into account conventional complexation of metal cations and competing reactions that extract H_2O [5] and HNO_3 [3], *i.e.*,

$$\begin{aligned}
UO_2^{2+} + 2NO_3^- + 2\overline{TBP} &\longleftrightarrow \overline{UO_2(NO_3)_2 \bullet 2TBP}\\
NpO_2^{+} + NO_3^- + 2\overline{TBP} &\longleftrightarrow \overline{NpO_2(NO_3) \bullet 2TBP}\\
Ga^{3+} + 3NO_3^- + 2\overline{TBP} &\longleftrightarrow \overline{Ga(NO_3)_3 \bullet 2TBP}\\
\vdots \quad + \quad \vdots &\longleftrightarrow \vdots \quad + \quad \vdots\\
H^+ + NO_3^- + \overline{TBP} &\longleftrightarrow \overline{HNO_3 \bullet TBP}\\
H^+ + NO_3^- + 2\,\overline{TBP} &\longleftrightarrow \overline{HNO_3 \bullet 2TBP}\\
\vdots \quad + \quad \vdots &\longleftrightarrow \vdots \quad + \quad \vdots\\
H_2O + \overline{TBP} &\longleftrightarrow \overline{H_2O \bullet TBP}\\
6H_2O + \overline{3TBP} &\longleftrightarrow \overline{6H_2O \bullet 3TBP}\\
\vdots \quad + \quad \vdots &\longleftrightarrow \vdots \quad + \quad \vdots,
\end{aligned}$$

where the complexation of H_2O and HNO_3 at a high nitric acid concentration generates larger extracted complexes [6, 8, 9]. The complete mechanism adds 30 reactions and 30 species to the overall system.

The degradation of the diluent and the solvent extractant species via radiolysis and hydrolysis processes is of interest in the formation of derived organic substances in both liquid and vapor phases. This is a particularly challenging area wherein models have not been sufficiently advanced and validated. Therefore, our objective is to assemble a reasonable prototype for the reaction mechanism to allow for computational simulations and future validation against experimental measurements. Although most of the direct radiation energy in the liquid phase is absorbed by the diluent (dodecane), the radiolysis products tend to be higher molecular weight alkanes (polymers) less prone to decomposition than the ligand [11]. Hence at the moment, we focus attention on the ligand, TBP, which suffers both hydrolysis and radiolysis. The latter is ignored in the current model as we address the former. Exposure to the radiolysis product of nitric acid, $^{\bullet}NO_3$, and nitric acid leads to dealkylation reactions [10, 4] of TBP producing dibutylphosphoric acid and monobutylphosphoric acid; a few representative reactions are:

$$\begin{aligned}
{}^{\bullet}NO_3 + \overline{TBP} &\xrightarrow{k_{19}} \overline{(C_4H_9O)_2({}^{\bullet}C_4H_8O)PO} + HNO_3\\
\vdots \quad + \quad \vdots &\longleftrightarrow \vdots \quad + \quad \vdots\\
H^+ + NO_3^- + \overline{TBP} &\xrightarrow{k_2} \overline{HDBP} + C_4H_9ONO_2\\
\vdots \quad + \quad \vdots &\longleftrightarrow \vdots \quad + \quad \vdots\\
H^+ + NO_3^- + HDBP &\xrightarrow{k_6} H_2MBP + C_4H_9ONO_2\\
\vdots \quad + \quad \vdots &\longleftrightarrow \vdots \quad + \quad \vdots
\end{aligned}$$

producing alkyl nitrates, nitrated phosphates, butanol, and butaldehyde; we also make assumptions of alkyl nitrates partitioning into the vapor phase as this information is unavailable [12].

The vapor phase kinetic model is contrived at this point to entail a mass transfer model for the underlying vapor-liquid equilibrium between the aqueous and vapor phases. It is unclear at the moment how to propose kinetics models of the interfacial mass transfer from the organic phase to the vapor phase (this is a work in progress). We have implemented 10 aqueous/vapor interfacial mass transfer reactions based on the equilibrium of species with known Henry's constant, for example:

$$\begin{aligned}
N_2O_{(aq)} &\xleftrightarrow{H_{N_2O}} N_2O_{(vap)}\\
NO_{(aq)} &\xleftrightarrow{H_{NO}} NO_{(vap)}\\
N_2O_{4(aq)} &\xleftrightarrow{H_{N_2O_4}} N_2O_{4(vap)}\\
\vdots \quad + \quad \vdots &\longleftrightarrow \vdots \quad + \quad \vdots
\end{aligned}$$

where the equilibrium values drive the mass transfer flux based on the relaxation constant to equilibrium; relaxation constants lump the effects of mixing and interfacial area.

The current reaction mechanism includes 152 reactions (118 aqueous phase, 24 aqueous/organic interface, and 10 aqueous/vapor) and 98 species (67 aqueous, 21 organic, 10 vapor). The system of ordinary differential equations representing mass balance in a closed control volume yields

$$d_t(\rho_{z,\alpha}) = \mathcal{R}_{z,\alpha}, \tag{1}$$

for each species z in phase α where the right side vector (species production rates) is computed from the reaction rates vector $\boldsymbol{r}$ as

$$\boldsymbol{R} = \boldsymbol{S}^{\mathsf{T}}\boldsymbol{r}$$

using the framework provided by `Cortix` [1].

RESULTS AND ANALYSIS

This work includes the implementation and testing of various initial concentration conditions for the numerical solution of (1). It is challenging to assemble these reactions into a combined mechanism and collect kinetics (rate constants and activation energies) data, as well as equilibrium constant data that allow for a robust solution of the ordinary differential equation (ODE) system. Our implementation allows for a flexible extension of the reaction mechanism and variation of parameters. The implementation using Cortix [1] is aimed at providing a framework to create a complex system of reaction kinetics including a large set of isotopes, typically computed from a used nuclear fuel depletion simulation. The following results use, among various parameters, dose rate density (power density) $D_\rho = 5\ \mathrm{J\,L^{-1}\,s^{-1}}$ where the species yield is computed as $\mathcal{Y}_z = G_z\, D_\rho\ \mathrm{mol\,dm^{-3}\,s^{-1}}$, nitric acid concentration $[HNO_3] = 2.5\ \mathrm{mol\,dm^{-3}}$, TPB/dodecane volume fraction, 30 %, temperature $T = 40\ ^\circ\mathrm{C}$, pressure $P = 1$ bar, and initial relative humidity 15 %.

Aqueous Phase

The initial condition in the aqueous phase is representative of being loaded with Pu^{4+}, NpO_2^{2+} and NpO_2^{+}. Hydroxylammonium nitrate is used to reduce Pu^{4+} to Pu^{3+} and hydrazinium

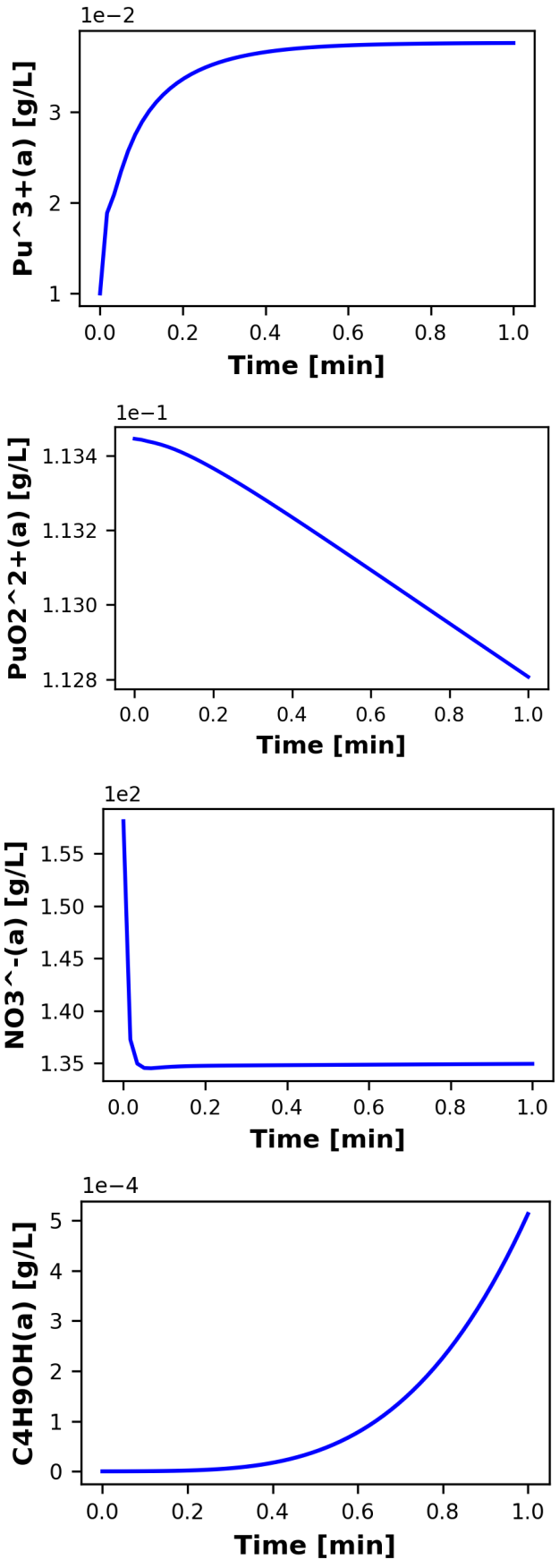

Fig. 1. Examples of simulated species concentration in the aqueous phase; bottom plot shows butanol as a degradation product of TPB.

used to reduce the concentration of nitrous acid. As an example, butanol generated in the organic phase by hydrolysis of TBP partitions into the aqueous phase (fig. 1).

Organic Phase

From the foregoing, the organic phase extracts the remaining Pu^{4+}, NpO_2^{2+} and NpO_2^{+} as complexes hence nitrate ions are consumed extensively (fig. 1). As an example of TPB degradation, the butanal species concentration in the organic phase is presented (fig. 2).

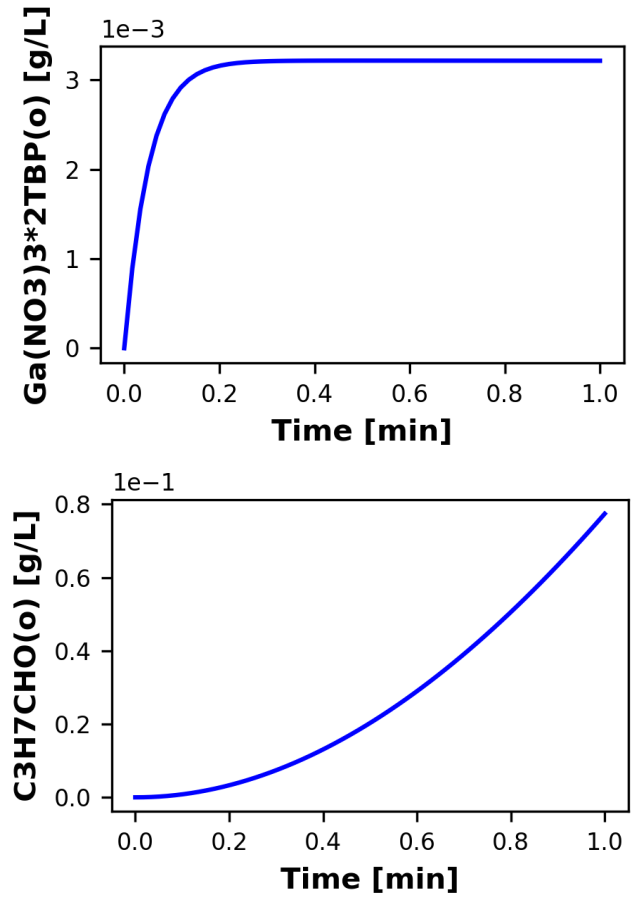

Fig. 2. Examples of simulated species concentration in the organic phase; bottom plot shows butanal as a degradation product of TPB.

Vapor Phase

Various nitrate volatiles are produced in the vapor phase. Other species of interested may be obtained by proposing mechanisms of interfacial mass transfer based on relaxation to equilibrium concentration. The objective of the present work was to implement and test a flexible and generic simulation framework.

CONCLUSIONS

It is clear that developing extensive kinetic mechanisms for nuclear solvent extraction processes is a challenging task. We have combined stand-alone mechanisms into a framework to aid experimental investigations. In particular, validation of mechanisms can be made more systematic when a flexible computational tool is available. Furthermore, the solution method using existing robust ODE solvers (SUNDIALS [13] and Scipy [14]) has proven robust, greatly simplifying the programming task at hand. Future work will be aimed at automating much of the implementation of reaction mechanisms as well as the assembly of multiple separation stages.

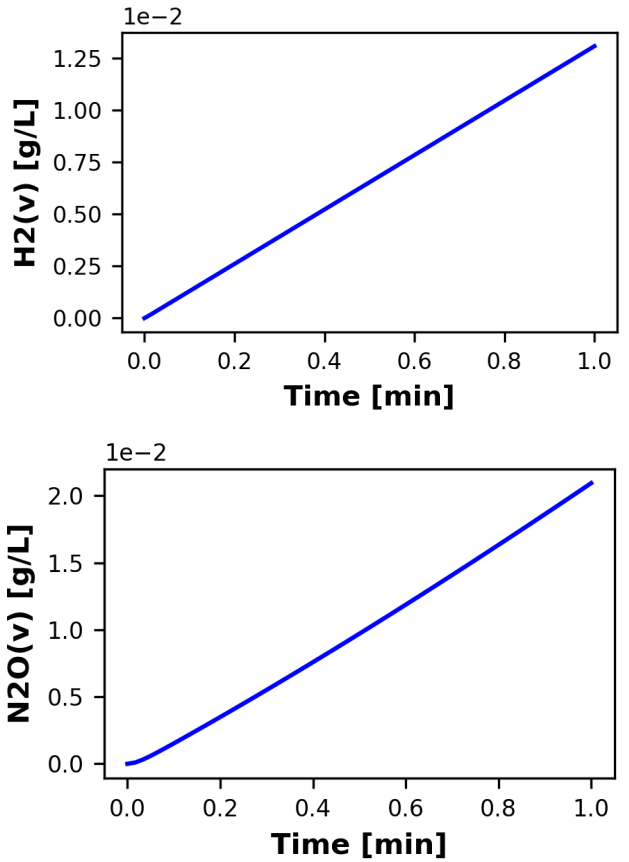

Fig. 3. Examples of simulated species concentration in the vapor phase. There is extensive water mass transfer into the vapor; not shown here.

ACKNOWLEDGMENTS

This work was supported by the Laboratory Director's Research and Development program of the Idaho National Laboratory for the US Department of Energy under contract DE-AC07-05ID14517, and the University of Massachusetts Lowell research program of the Francis College of Engineering.

REFERENCES

1. CORTIX DEVELOPMENT TEAM, "Cortix Manual," https://cortix.org (2019), downloadable at https://cortix.org at the time of publication. Revision Jan. 2019.
2. R. C. CRIPPS, B. JÄCKEL, and S. GÜNTAY, "On the radiolysis of iodine, nitrate and nitrite ions in aqueous solution: An experimental and modeling study," *Nucl. Eng. Des.*, **241**, 3333–47 (2011).
3. Y. KATSUMURA, P. Y. JIANG, R. NAGAISHI, T. OISHI, and K. ISHIGURE, "Pulse Radiolysis Study of Aqueous Nitric Acid Solutions. Formation Mechanism, Yield, and Reactivity of NO_3 Radical," *J. Phys. Chem.*, **95**, *11*, 4435–39 (1991).
4. B. J. MINCHER, G. MODOLO, and S. P. MEZYK, "Review Article: The Effects of Radiation Chemistry on Solvent Extraction: 1. Conditions in Acidic Solution and a Review of TBP Radiolysis," *Solvent Extr. Ion Exch.*, **27**, 1–25 (2009).
5. S. TACHIMORI, "Numerical Simulation for Chemical Reactions of Actinide Elements in Aqueous Nitric Acid Solution," *J. Nucl. Sci. Technol.*, **28**, 218–27 (1991).
6. W. S. GROENIER, "Technical Manual for SEPHIS Mod4, Version 2.11," Technical Manuscript ORNL/TM-11589, Oak Ridge National Laboratory, Tennessee, TN 37831-6181, U.S.A. (Feb. 1991).
7. T. ISHIMORI and K. WATANABE, "Inorganic Extraction Studies on the System of Tri-*n*-butyl Phosphate–Nitric Acid," *Bull. Chem. Soc. Jpn.*, **33**, 1443–8 (1960).
8. H. NAGANAWA and S. TACHIMORI, "Hydration and Dimerization of Tributyl Phosphate in Dodecane," *Anal. Sci.*, **10**, 309–14 (1994).
9. H. NAGANAWA and S. TACHIMORI, "Hydration and Dimerization of Tributyl Phosphate in Dodecane," *Anal. Sci.*, **10**, 607–13 (1994).
10. K. L. NASH, P. G. RICKERT, and E. P. HORWITZ, "Degradation of TRUEX-Dodecane Process Solvent," *Solvent Extr. Ion Exch.*, **7**, *4*, 655–75 (1989).
11. B. J. MINCHER and S. P. MEZYK, "Radiation chemical effects on radiochemistry: A review of examples important to nuclear power," *Radiochim. Acta*, **97**, 519–34 (2009).
12. D. R. PETERMAN, L. G. OLSON, G. S. GROENEWOLD, R. G. MCDOWELL, R. D. TILLOTSON, and J. D. LAW, "Characterization of Radiolytically Generated Degradation Products in the Strip Section of a TRUEX Flowsheet," Technical Report FCRD-SWF-2013-000202 INL/EXT-13-29727, Idaho National Laboratory (Aug. 2013).
13. SUNDIALS DEVELOPMENT TEAM, "SUNDIALS: SUite of Nonlinear and DIfferential/ALgebraic Equation Solvers," https://computation.llnl.gov/projects/sundials (2019), downloadable online, at the time of publication. Revision Jan. 2019.
14. SCIPY DEVELOPMENT TEAM, "Scientific Python Library," https://www.scipy.org/ (2019), downloadable online, at the time of publication. Revision Jan. 2019.